三相脉宽调制整流器的约束预测控制

刘　佳, 张立炎, 陈启宏†, 钱　立, 全书海
(武汉理工大学 自动化学院, 湖北 武汉 430070)

摘要: 本文将基于并行神经网络优化的约束模型预测控制(MPC)应用于脉宽调制(PWM)整流器中, 提高了电网的质量. 在三相静止坐标系下, 建立了三相PWM整流器的解耦数学模型, 采用约束模型预测控制策略, 突破了有限集和无约束条件下预测控制的局限性. 为了提高单步优化的速度, 采用神经网络优化算法求解模型预测控制的在线优化. 在保证系统单位功率因数的前提下, 当系统负载突然变化时, 具有快速动态响应稳定输出直流电压的性能. 采用FPGA控制器实现并行计算, 减少了预测控制算法的计算时间. 最后, 通过仿真和实验结果得到, 采用本文的控制策略, 总谐波失真(THD)降低了2.5%, 达到稳态的时间大约是PI 控制算法的五分之一, 为12 ms, 验证了该方法的可行性和有效性.

关键词: 三相脉宽调制整流器; 模型预测控制; 单位功率因数; 神经网络优化
引用格式: 刘佳, 张立炎, 陈启宏, 等. 三相脉宽调制整流器的约束预测控制. 控制理论与应用, 2019, 36(3): 399 – 407
DOI: 10.7641/CTA.2018.80481

Constrained model predictive control for a three-phase pulse width modulation rectifier

LIU Jia, ZHANG Li-yan, CHEN Qi-hong†, QIAN Li, QUAN Shu-hai
(School of Automation, Wuhan University of Technology, Wuhan Hubei 430070, China)

Abstract: In this paper, constrained model predictive control (MPC), based on parallel neural network optimization, is proposed to apply to pulse width modulation (PWM) rectifier and improve power quality. A decoupled model of three-phase rectifier under three-phase stationary coordinates system is built. Then, this constrained MPC method breaks the limits of predictive control with finite set and without constraints. Neural network optimization is used to solve online optimization of MPC and accelerate single step optimization. This method is proposed to guarantee unity power factor, which also provides a regulated output DC–voltage with fast dynamics response against sudden changes in the load. A FPGA controller is employed to implement parallel calculation so as to reduce the computation time on predictive control algorithm. Simulation and experimental results are compared to verify effectiveness and feasibility of the proposed method. The measured total harmonic distortion (THD) is 2.5% lower and the time to reach steady state is 12ms, which is almost one fifth of PI control.

Key words: three-phase PWM rectifier; model predictive control; unity power factor; neural network optimization
Citation: LIU Jia, ZHANG Liyan, CHEN Qihong, et al. Constrained model predictive control for a three-phase pulse width modulation rectifier. *Control Theory & Applications*, 2019, 36(3): 399 – 407

1 Introduction

Along with shortage of petroleum energy and serious environmental pollution problems, electric vehicles (EVs) and plug-in hybrid electric vehicles (PHEVs), as a low-carbon way to travel, has drawn the attention of researches and customers. However, massive harmonics is brought to the power grid by EVs and their chargers. The three-phase pulse width modulation (PWM) rectifier, also referred to as AC/DC converter belonging to charge equipment, has been successfully applied to guarantee unity power factor[1–2].

Many control strategies have been investigated for three-phase PWM rectifier. The controller with the characteristic of fast dynamic response and high control precision, is essential to improve power quality and decrease the harmonics interference. The decoupling control of active power and reactive power of three-phase PWM rectifier is realized with double closed-loop control structure[3]. An appropriate controller should be implemented in this situation, while traditional PID control algorithm is hard to meet this requirement. Taking constraints on state variables, manipulated variables and output variables into account, model predictive control (MPC) could explicitly optimize closed-loop performance. Then, this method has drawn significant attention of power electronics researchers[4–5].

A three-phase unity power factor rectifier based on MPC with variable hysteresis current control based on

Received 29 June 2018; accepted 25 November 2018.
†Corresponding author. E-mail: qh_chen@hotmail.com; Tel.: +86 13659812012.
Recommended by Associate Editor: SU Mei.
Supported by the National Nature Science Foundation of China (61673306).

three-phase stationary coordinate system is proposed[6]. Model predictive control is used in marine electric power plant and wind energy conversion systems[7–8]. A recurrent neural network method for solving convex quadratic program is proposed[9]. The model predictive control for PWM rectifier based on two-phase rotating dq coordinate system is investigated[10]. A fixed frequency model predictive control method for three-phase PWM rectifier is proposed[11–12]. Two weight coefficients are added in cost function[13–14]. The optimized weight factor of the cost function is essential[15]. A model predictive direct power control of the three-phase PWM rectifier is proposed[16–17].

However, the above MPC methods for the rectifier based on finite control set are MPCs without constraints. Due to no constraints, these methods have some shortcomings, such as easy to go out of bounds, large fluctuation of control variables and large output deviation. As a result, it is difficult to guarantee high quality of the power from the grid while current tracking error can't be small as expected. In this paper, constrained MPC is proposed to track mixed signal precisely. Control precision and performance will be improved while duty ratio of each switch has been controlled as a continuous variable in the range of $[0, 1]$.

This paper is organized as follows. In Section 2, the decoupled model and predictive model of the three-phase PWM rectifier under three-phase stationary coordinates system are built. The constrained MPC strategy is proposed to optimize duty ratio of each switch of three-phase PWM rectifier in Section 3. Section 4 introduces simulation and experiment results. Finally, Section 5 concludes this paper.

2 Model of the rectifier

The topology of the three-phase rectifier is shown in Fig. 1. As we can see, there are 6 power switches in the rectifier, which are named as $S_1 - S_6$. $e_{\rm a}, e_{\rm b}$, and $e_{\rm c}$ are grid voltages, $i_{\rm a}, i_{\rm b}$, and $i_{\rm c}$ are grid currents.

The filter inductors L transmit energy and R is the equivalent resistor of the inductors L. The output of the rectifier are load resistance $R_{\rm L}$ in parallel with capacitor C which is equivalent to two capacitor 2C in series. $V_{\rm o}$ is the output DC voltage of the rectifier, and i_0 is the output current of the rectifier.

Obviously, three-phase voltages, three-phase currents and control variables couple each other in model of the rectifier. In order to simplify the modelling complexity, it is practical to suppose that the three-phase power grid is working under a balanced condition. Then, it can be separated into three single-phase independent circuits while neutral points N and n are at the same potential.

The circuit illustrated in Fig. 1 was simulated using bipolar sinusoidal pulse width modulation under a switching frequency of 20 kHz, result in a output DC voltage is 600 V. Fig. 2 shows that the instantaneous voltage between the reference point N and n is not zero and the voltage amplitude is half of the DC voltage. However, the average value of $V_N n$ is zero in a switching period, the reference points N and n of the system are considered at the same potential.

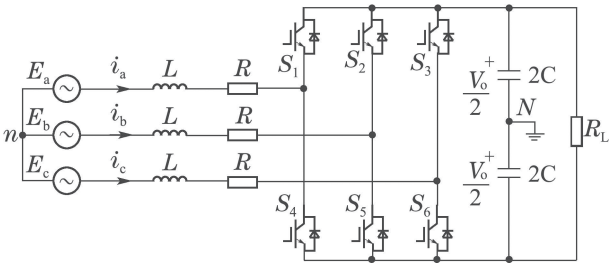

Fig. 1 Topology of the three-phase rectifier

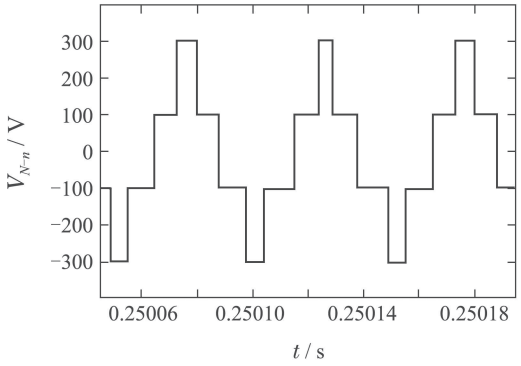

Fig. 2 Instantaneous voltage between the point N and n

The decoupled model of the system are shown in Fig. 3. According to Kirchhoff's law of voltage and current, mathematical model of the rectifier can be described as the following equations.

$$\begin{cases} L\dfrac{{\rm d}i_{\rm a}}{{\rm d}t} = e_{\rm a} - Ri_{\rm a} - V_{\rm o}u_{1{\rm a}}, \\ L\dfrac{{\rm d}i_{\rm b}}{{\rm d}t} = e_{\rm b} - Ri_{\rm b} - V_{\rm o}u_{1{\rm b}}, \\ L\dfrac{{\rm d}i_{\rm c}}{{\rm d}t} = e_{\rm c} - Ri_{\rm c} - V_{\rm o}u_{1{\rm c}}, \end{cases} \tag{1}$$

$$C\frac{{\rm d}V_{\rm o}}{{\rm d}t} = i_{\rm a}u_{\rm a} + i_{\rm b}u_{\rm b} + i_{\rm c}u_{\rm c} - i_{\rm o}, \tag{2}$$

where $u_{\rm a}, u_{\rm b}, u_{\rm c} \in [0, 1]$ denote duty cycle of switches of the legs, A, B, and C, respectively. $u_{1{\rm a}} = u_{\rm a} - \dfrac{1}{2}$, $u_{1{\rm b}} = u_{\rm b} - \dfrac{1}{2}$, $u_{1{\rm c}} = u_{\rm c} - \dfrac{1}{2}$, $u_{1{\rm a}}, u_{1{\rm b}}, u_{1{\rm c}} \in [-\dfrac{1}{2}, \dfrac{1}{2}]$.

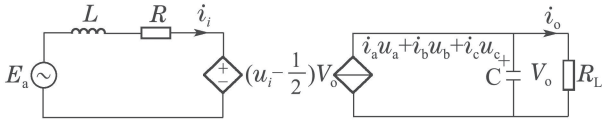

Fig. 3 The decoupled equivalent per-phase circuit of the rectifier N and n

The voltage $V_{\rm o}$ is a variable value while working under the steady state, but it can be considered as a constant value in one control cycle. Continuous model of the rectifier can be written in state-space form as

$$\frac{{\rm d}i}{{\rm d}t} = Ai + Bu + Ne_{\rm g}, \tag{3}$$

where

$$i=(i_{\rm a}\ i_{\rm b}\ i_{\rm c})^{\rm T},\ u=(u_{1{\rm a}}\ u_{1{\rm b}}\ u_{1{\rm c}})^{\rm T},\ e_{\rm g}=(e_{\rm a}\ e_{\rm b}\ e_{\rm c})^{\rm T},$$
$$A=-\frac{R}{L}E,\ B=-\frac{V_{\rm o}}{L}E,\ N=\frac{1}{L}E,$$
$$E=\begin{bmatrix}1&0&0\\0&1&0\\0&0&1\end{bmatrix}.$$

Digital implementation of the predictive control requires discrete-time model. The continuous-time model (3) is described as

$$i(k+1) = Gi(k) + Hu(k) + We_{\rm g}(k), \tag{4}$$

where $G={\rm e}^{AT_{\rm s}}$, $H=\int_0^{T_{\rm s}}{\rm e}^{At}B{\rm d}t$, $W=\int_0^{T_{\rm s}}{\rm e}^{At}N{\rm d}t$, and $T_{\rm s}$ is the control period.

Prediction horizon P and control horizon M are two essential parameters in MPC. The prediction horizon determines how long will the controller takes to predict the behavior of the rectifier until computing an optimal control. The control horizon determines how long will the controller takes to update prediction of the control variables. They are chosen to get a good trade-off between performance and computation time.

The predictive model of the rectifier can be written as

$$I(k) = \Psi i(k) + \Theta U(k) + \Lambda E_{\rm g}(k), \tag{5}$$

where

$$I(k)=\begin{bmatrix}(i(k+1|k)\\ \vdots\\ i(k+P|k)\end{bmatrix}_{P\times 1},\Psi=\begin{bmatrix}G\\ \vdots\\ G^p\end{bmatrix}_{P\times 1},$$
$$U(k)=\begin{bmatrix}u(k)\\ \vdots\\ u(k+M-1)\end{bmatrix}_{M\times 1},$$
$$E_{\rm g}(k)=\begin{bmatrix}e_{\rm g}(k)\\ \vdots\\ e_{\rm g}(k+M-1)\end{bmatrix}_{M\times 1},$$
$$\Theta=\begin{bmatrix}H&0&s&0\\ GH&H&s&0\\ \vdots&\vdots&\ddots&\vdots\\ G^{P-1}H&G^{P-2}H&s&G^{P-M}H\end{bmatrix}_{P\times M},$$
$$\Lambda=\begin{bmatrix}W&0&s&0\\ GW&W&s&0\\ \vdots&\vdots&\ddots&\vdots\\ G^{P-1}W&G^{P-2}W&s&G^{P-M}W\end{bmatrix}_{P\times M}.$$

3 Predictive control of the rectifier

In this paper, the controller, proposed to guarantee unit power factor and a stable regulated voltage, consists of a fast-inner input-current loop and a outer-voltage loop. The outer-voltage loop computes the reference value of the input current and the inner-current loop is built to achieve fast current tracking between reference input current and real input current.

3.1 Predictive control strategy

MPC is usually used to predict output trajectory of a process and compute a series of control actions, by minimizing the error between the predicted trajectory and desired trajectory. The predictive control strategy is proposed to minimize current tracking errors between reference input current and real input current of the rectifier. The cost function is defined as following:

$$V(k) = [I^*(k)-I(k)]^{\rm T}Q[I^*(k)-I(k)] + U(k)^{\rm T}RU(k), \tag{6}$$

where

$$I^*(k)=(i^*(k+1)\cdots i^*(k+P))^{\rm T}_{P\times 1},$$
$$i^*(k+i)=(i^*_{\rm a}(k+i)\ \ i^*_{\rm b}(k+i)\ \ i^*_{\rm c}(k+i))^{\rm T}.$$

Substituting (5) into (6)

$$V(k)=\frac{1}{2}U^{\rm T}(k)\Phi U(k)+f^{\rm T}U(k)+m, \tag{7}$$

where

$$\Phi=2(\Theta^{\rm T}Q\Theta+R),\ \Gamma=\Psi i(k)+\Lambda E_{\rm g}(k),$$
$$f^{\rm T}=-2[I^*(k)-\Gamma]^{\rm T}Q\Theta,$$
$$m=[I^*(k)-\Gamma]^{\rm T}Q[I^*(k)-\Gamma].$$

Because m is a constant in one control cycle, it can be ignored to solve quadratic program. The cost function can be obtained in quadratic program form:

$$\begin{cases}\min F(U)=\dfrac{1}{2}U^{\rm T}\Phi U+f^{\rm T}U,\\ {\rm s.t.}-\dfrac{1}{2}\leqslant U\leqslant\dfrac{1}{2}.\end{cases} \tag{8}$$

3.2 Fast optimization algorithm

In this paper, predictive control based on the state-space average model can eventually be transformed into solving the quadratic program (QP) problem. Since the cost function (8) is a convex quadratic program, it is important to choose an appropriate optimization algorithm to guarantee the rapidity of the computation.

3.2.1 Recurrent neural network algorithm

The recurrent neural network (RNN) method is chosen to deal with convex quadratic program is proposed[8]. The optimization algorithm can guarantee that control variables converge rapidly in the limited time and improve the stability of system.

The Lagrangian function of (8) can be expressed as

$$L(U,\delta,\eta)=\frac{1}{2}U^{\rm T}\Phi U+f^{\rm T}U-\delta^{\rm T}(U-\eta). \tag{9}$$

According the saddle point theorem, the optimal solution of (8) satisfies

$$\begin{cases} \eta = U, \\ U = P_{\rm u}(\eta - \delta), \\ \Phi U + f - \delta = 0. \end{cases} \tag{10}$$

Equation (10) can be rewritten as:

$$\begin{cases} W_{\rm c}\delta + l = P_{\rm u}(W_{\rm c} + l - \delta), \\ U = W_{\rm c}\delta + l, \end{cases} \tag{11}$$

where

$$\begin{aligned} &W_{\rm c} = \Phi^{-1},\ \ l = -\Phi^{-1}f, \\ &P_{\rm u}(x_i) = [P_{\rm u}(x_1)\ \ P_{\rm u}(x_2)\ \ \cdots\ \ P_{\rm u}(x_m)]^{\rm T}, \\ &\qquad i = 1, 2, \cdots, m, \\ &P_{\rm u}(x_i) = \begin{cases} 0, & x_i < 0, \\ x_i, & 0 \leqslant x_i \leqslant 1, \\ 1, & x_i > 1. \end{cases} \end{aligned}$$

The single-layer RNN method is used to solve (10). The dynamic equation is as follows:

$$\begin{cases} \dfrac{{\rm d}\delta}{{\rm d}t} = \theta[P_{\rm u}(W_{\rm c}\delta + l - \delta) - W_{\rm c}\delta - l], \\ U(t) = W_{\rm c}\delta(t) + l. \end{cases} \tag{12}$$

According (12), we get stable value of δ, predictive controller with single-layer neural network computation is designed to find optimal solution of U.

3.2.2 Stability analysis of RNN

Proof 1 In order to prove that the state trajectory of RNN converges to δ^*, the Lyapunov function is displayed as follow:

$$V = \frac{1}{2}\|G(\delta - \delta^*)\|^2, \tag{13}$$

where the G is a symmetrical positive determined matrix, which gives

$$G^2 = I + W_{\rm c}.$$

Then derivation of the Lyapunov function can be written as

$$\frac{{\rm d}V}{{\rm d}t} = (\delta - \delta^*)^{\rm T}G^2\theta\{P_{\rm u}(W_{\rm c}\delta + l - \delta) - W_{\rm c}\delta - l\}.$$

From (10) and (12), we obtain

$$\begin{aligned} &\{P_{\rm x}(W\lambda + q - \lambda) - W\lambda^* - q\}^{\rm T} \times \\ &\{(\lambda^* - \lambda) - P_{\rm x}(W\lambda + q - \lambda) + W\lambda + q\} \geqslant 0. \end{aligned}$$

Thus, we have

$$\begin{aligned} &(\lambda - \lambda^*)(I + W)\{P_{\rm x}(W\lambda + q - \lambda) - \\ &W\lambda - q\} \leqslant -(\lambda - \lambda^*)^{\rm T}W(\lambda - \lambda^*) - \\ &\|P_{\rm x}(W\lambda + q - \lambda) - W\lambda - q\|^2 \leqslant 0. \end{aligned}$$

Therefore, $\dfrac{{\rm d}V}{{\rm d}t} \leqslant 0$, resulting in the system converges to a stable state.

Proof 2 In order to prove that RNN can converge in a finite time in each sampling time, giving

$$\begin{aligned} &f(\lambda(t)) = \\ &\|P_{\rm x}(W\lambda(t) + q - \lambda(t)) - W\lambda(t) - q\|^2, \end{aligned} \tag{14}$$

where $\delta(t)$ obtains the state trajectory of (12), thus, we have $f(\delta(t)) \geqslant 0$, $f(\delta(t_0)) > 0$. Because $f(\delta(t))$ is continuous, there are $\tau > 0$ and $\lambda < 0$ satisfying for arbitrary $t \in [t_0, t + \tau]$, resulting in $f(\delta(t)) \geqslant \lambda$. According to Proof 1, we obtain

$$\frac{{\rm d}V}{{\rm d}t} \leqslant -\theta\|P_{\rm u}(W_{\rm c}\delta + l - \delta) - W_{\rm c}\delta - l)\|^2.$$

Therefore, we have

$$\begin{aligned} &V(\lambda(t)) \leqslant \\ &V(\lambda(t_0)) - \mu\int_{t_0}^{t}\|P_{\rm x}(W\lambda(s) + q - \\ &\lambda(s)) - W\lambda(s) - q)\|^2{\rm d}s \leqslant \\ &(V(\lambda(t_0)) - \mu\int_{t_0}^{t_0+\tau}\|P_{\rm x}(W\lambda(s) + q - \\ &W\lambda(s) - q)\|^2{\rm d}s = \\ &V(\lambda(t_0)) - \mu\int_{t_0}^{t_0+\tau} f(\lambda(s)){\rm d}s \leqslant \\ &V(\lambda(t_0)) - \mu\delta\tau, \end{aligned}$$

where $\theta = V(\delta(t_0))/(\tau\lambda)$, if $t \geqslant t_0 + \tau$, we obtain

$$V(\delta(t)) \leqslant V(\delta(t_0)) - \theta\lambda\tau = 0.$$

Therefore, as long as the δ could be large enough, the problem (8) can converge in a limited time in each sampling time.

3.2.3 Comparing of optimization algorithms

In order to improve dynamic and stable performance, several algorithms have been proposed to solve the QP problem, such as fast gradient method (FGM)[18], alternating direction method of multipliers (ADMM)[19] and RNN. A simulation circuit has been built in Simulink and the three optimal algorithms are programmed by using S-function module, receptivity. At the same time, they are working under the same P and Q parameters. In order to compare the computing speed of three algorithms, tic and toc instructions are added before and after the each small cycle, receptivity, to record the number of single-step small cycles, one-step optimization time and the total time when the system reaches steady state. And the recorded data is shown in Table 1.

Table 1 Comparing the computing speed of optimization algorithms

Algorithm	FGM	RNN	ADMM
The number of small cycle	8	4	26
Maximum time for single-step optimization/ms	0.112	4.085	19.53
Minimum time for single-step optimization/ms	0.033	0.058	0.137
Total time to steady state/ms	20.03	8.950	30.42

The number of small cycle and the optimization time of small cycle have the greatest impact on the over-

all online computing time of the algorithm, while small cycles can only be executed serially in the FPGA. Compared with FGM and ADMM, the RNN has the characteristics of the least number of small cycles, the shortest time to reach steady state and the fastest on-line calculation speed. Then, the RNN is choose to implement in this paper.

3.3 Unity power factor rectifier

In order to achieve unity power factor, sinusoidal input currents should be in phase with the line voltages, then $i = ke_{\mathrm{g}}$. In order to linearize the output voltage dynamically, the amplitude control k is conceived. We assume that the reference input current by computing the value is k, and the value of k can be derived as follows:

$$\begin{cases} \varepsilon_{\mathrm{a}} = ke_{\mathrm{a}} - i_{\mathrm{a}}, \\ \varepsilon_{\mathrm{b}} = ke_{\mathrm{b}} - i_{\mathrm{b}}, \\ \varepsilon_{\mathrm{c}} = ke_{\mathrm{c}} - i_{\mathrm{c}}, \end{cases} \tag{15}$$

where $\dot{\varepsilon} = 0$, $\varepsilon = (\varepsilon_{\mathrm{a}}\ \varepsilon_{\mathrm{b}}\ \varepsilon_{\mathrm{c}})^{\mathrm{T}}$.

Substituting (1) and (2) into (15), we can obtain

$$C\frac{\mathrm{d}V_{\mathrm{o}}}{\mathrm{d}t} = \frac{k}{V_{\mathrm{o}}}(e_{\mathrm{a}}^2+e_{\mathrm{b}}^2+e_{\mathrm{c}}^2) - \frac{kL}{V_{\mathrm{o}}}\frac{\mathrm{d}k}{\mathrm{d}t}(e_{\mathrm{a}}^2+e_{\mathrm{b}}^2+e_{\mathrm{c}}^2) - \frac{k^2L}{V_{\mathrm{o}}}(e_{\mathrm{a}}\frac{\mathrm{d}e_{\mathrm{a}}}{\mathrm{d}t}+e_{\mathrm{b}}\frac{\mathrm{d}e_{\mathrm{b}}}{\mathrm{d}t}+e_{\mathrm{c}}\frac{\mathrm{d}e_{\mathrm{c}}}{\mathrm{d}t}) - i_{\mathrm{o}}, \tag{16}$$

where the grid voltages have a sinusoidal waveform defined by

$$\begin{cases} e_{\mathrm{a}} = V_{\mathrm{s}}\cos(w_0 t), \\ e_{\mathrm{b}} = V_{\mathrm{s}}\cos(w_0 t - \dfrac{2\pi}{3}), \\ e_{\mathrm{c}} = V_{\mathrm{s}}\cos(w_0 t - \dfrac{4\pi}{3}). \end{cases} \tag{17}$$

Substituting (17) in (16), the following equation is deduced.

$$C\frac{\mathrm{d}V_{\mathrm{o}}}{\mathrm{d}t} = \frac{3V_{\mathrm{s}}^2 k}{2V_{\mathrm{o}}} - i_{\mathrm{o}}. \tag{18}$$

In order to linearize the output voltage dynamically, the nonlinear control of k is proposed as follows:

$$k = \frac{2V_{\mathrm{o}}}{3V_{\mathrm{s}}^2}[k_{\mathrm{i}}\int_{-\infty}^{t}(V_{\mathrm{o}}^* - V_{\mathrm{o}})\mathrm{d}\tau + k_{\mathrm{p}}(V_{\mathrm{o}}^* - V_{\mathrm{o}}) + \frac{V_{\mathrm{o}}}{R_{\mathrm{L}}}]. \tag{19}$$

The calculation of the parameter k is obtained by PI control with feedforward control of the output voltage which can provide a regulated output DC–voltage with fast dynamics response against sudden changes in the load.

4 Simulation and experiment

In this section, effectiveness of the proposed constrained MPC strategy is verified by simulation in MATLAB/Simulink and experiment of rectifier. The parameters used in the simulation and experiment are given in Table 2.

4.1 Simulation

In order to verify the performance of the proposed constrained MPC method, a predictive controller was implemented of the three-phase PWM rectifier by MATLAB/Simulink based on the parameters given in Table 2. S–Function module is designed according to MPC to achieve the function of the predictive controller, and the circuit module and controller module form the entire simulation system.

Table 2 Parameters of the rectifier

Parameters	Description	Value
V_{o}	Output DC voltage	600 V
P_{e}	Rated power	10 kW
V_{g}	Grid RMS voltage	220 V
f_{n}	Grid frequency	50 Hz
T_{s}	Control period	50 μs
L	Filter inductance	3 mH
R	Equivalent resistor	0.1 Ω
C	Filter capacitance	1000 μF
R_{L}	Load resistor	36 Ω

Prediction horizon and control horizon directly affect not only the amount of calculation, but also rapidity and stability of the rectifier. A MPC with smaller P and larger M has greater rapidity and worse stability. On the contrary, larger P and smaller M will cause worse rapidity and greater stability. In this paper, P and M are set as 2 to gain good tradeoff between rapidity and stability. The weighting factors q and r are closely related to the tracing error and power quality. The guideline for weighting factors design proposed in [12] is used to select weighting factors. The weighting factors q and r is set as 6000 and 0.1, respectively, to gain good tradeoff and power quality. The simulation results of constrained MPC and PI controller are shown in Fig. 4 and Fig. 5.

In the simulations, the rectifier operated at rated power, and the reference DC voltage was 600 V. As shown in Fig. 4 and Fig. 5, the output DC voltage is 600 V with small steady-state error and the input current of each phase is almost 15 A. The input current keeps the same phase with the grid voltage, then the rectifier unit power factor operation function is achieved. But there are significant differences between two methods.

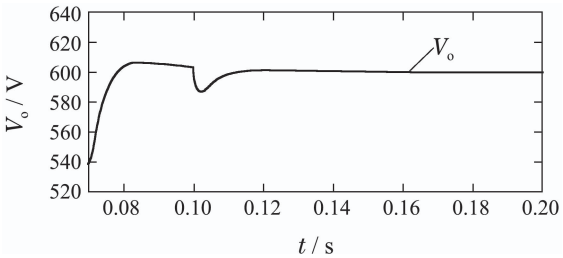

(a) Output DC voltage

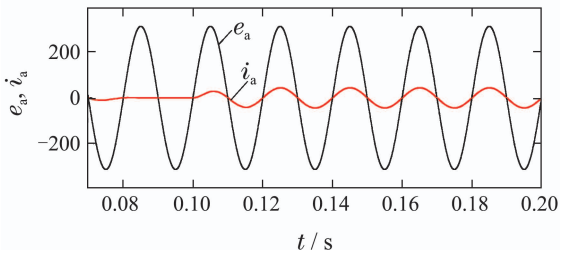

(b) Grid voltage e_a and input current i_a

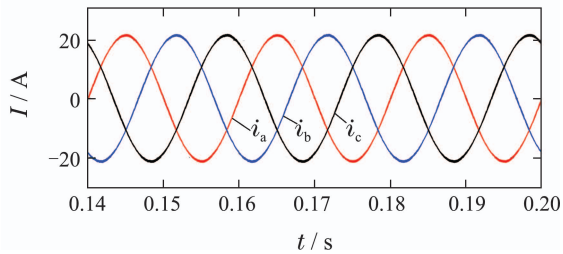

(c) Input current

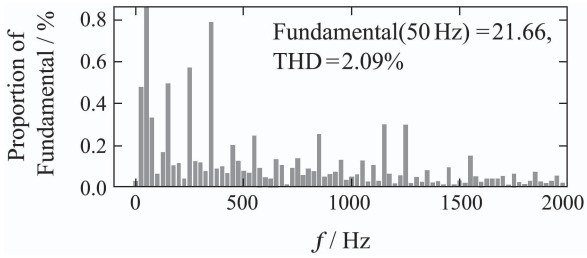

(d) FFT analysis of input current

Fig. 4 Simulation results of constrained MPC

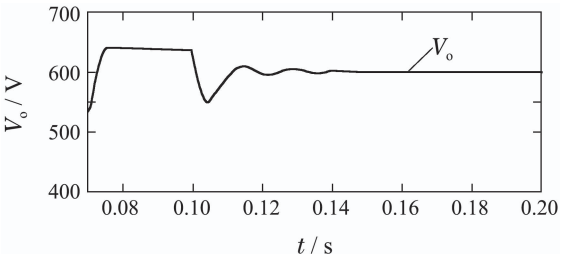

(a) Output DC voltage

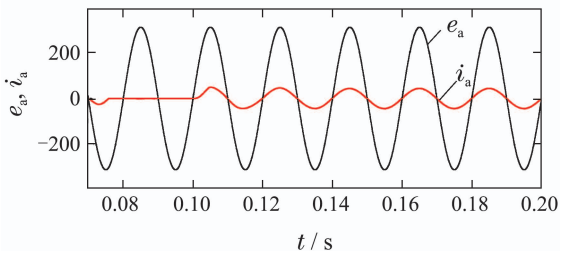

(b) Grid voltage e_a and input current i_a

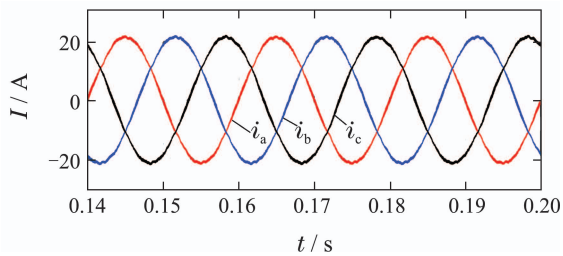

(c) Input current

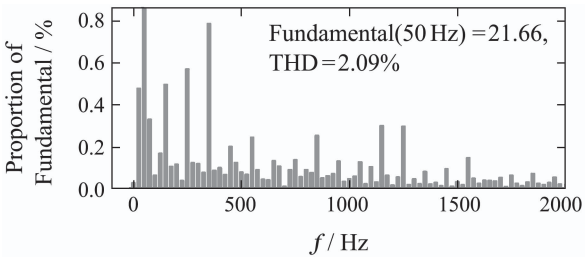

(d) FFT analysis of input current

Fig. 5 Simulation results of PI controller

Compared with PI controller, input current of constrained MPC is obviously smoother. What's more, constrained MPC reduces total harmonics distortion (THD) by 1.15% compared with PI controller. Hence, the constrained MPC strategy has a good performance in harmonics characteristic.

To get better comparison of dynamic performance of constrained MPC and PI, we changed reference D-C voltage in operation, and the output DC voltage is shown in Fig. 6 and Fig. 7. After changing the reference value, the time to reach steady state again of constrained MPC is 5 ms, which is much shorter than that of PI controller, about 25 ms. It demonstrates that the constrained MPC has better dynamic performance than PI controller.

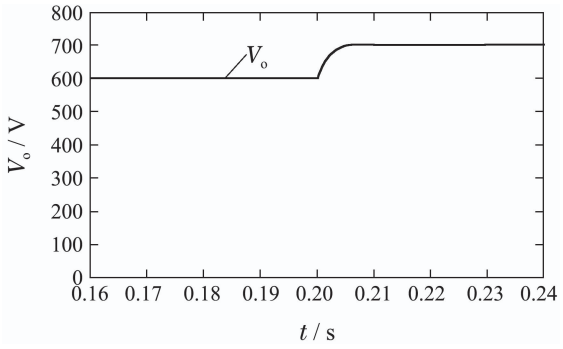

(a) Change reference DC voltage from 600 to 700

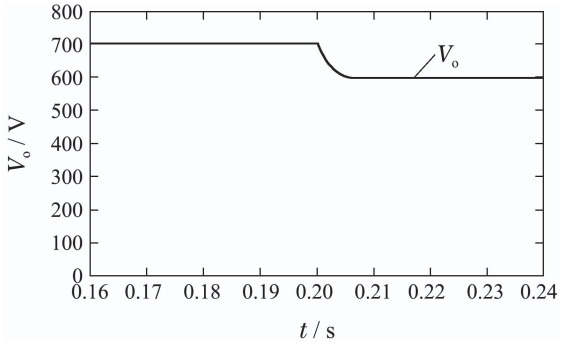

(b) Change reference DC voltage from 700 to 600

Fig. 6 Output DC voltage of constrained MPC

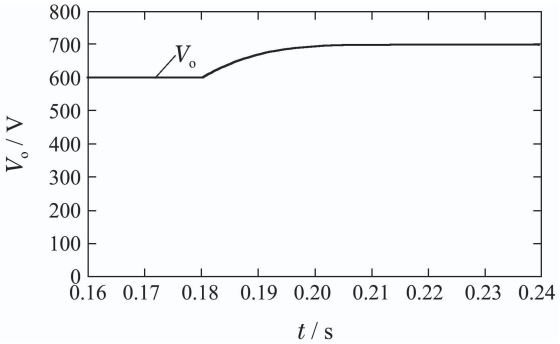

(a) Change reference DC voltage from 600 to 700

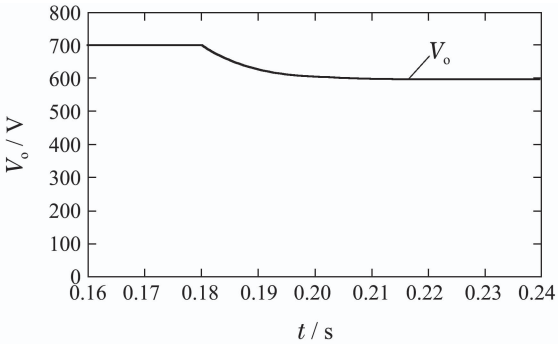

(b) Change reference DC voltage from 700 to 600

Fig. 7 Output DC voltage of PI controller

In conclusion, the constrained MPC strategy has lower THD and faster response speed.

4.2 Experiment

To further validate the feasibility of constrained MPC strategy, a three-phase PWM rectifier was setup according to Fig. 1 and Table 1. Infineon IGBTs were employed. FPGA with the ability of high-speed parallel calculation, is chosen as the controller to implement the real-time control algorithm. As shown in Fig. 8, the structure of FPGA controller consists of Read/Write Module, Parallel Computing Module and I/O ports. Time Control Module is built to control the whole state switches which are described as the state machine. And the MAC module is used to calculate the matrix value from the RAM and ROM. A sampling board with three-channel AC voltage sampling, three-channel AC current sampling and single-channel DC voltage sampling was connected the FPGA control board. Three driver modules were used to receive the PWM signals from FPGA, and drive the IGBTs. The experimental setups of rectifier is shown in Fig. 9.

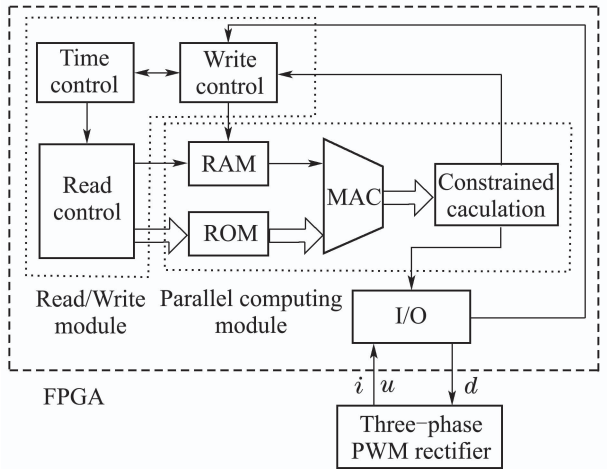

Fig. 8 The structure of FPGA controller

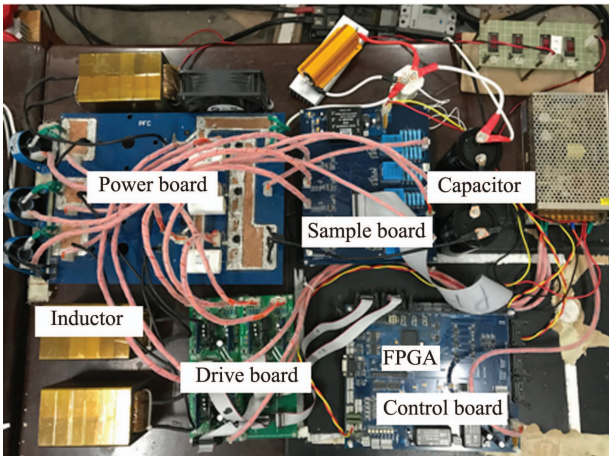

Fig. 9 Photographs of experimental setups of rectifier

Figures 10–13 are the experimental results of two strategies, respectively. The experimental result of constrained MPC and PI control are very similar to simulation results. The output DC voltage is 600 V with small steady-state error and the sinusoidal input current and the grid voltage of phase A are strictly in the same frequency phase.

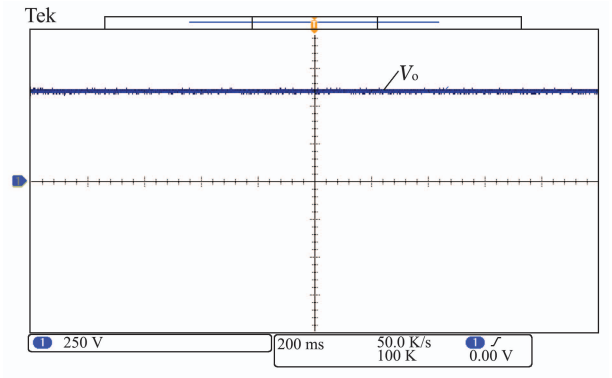

(a) Output DC voltage

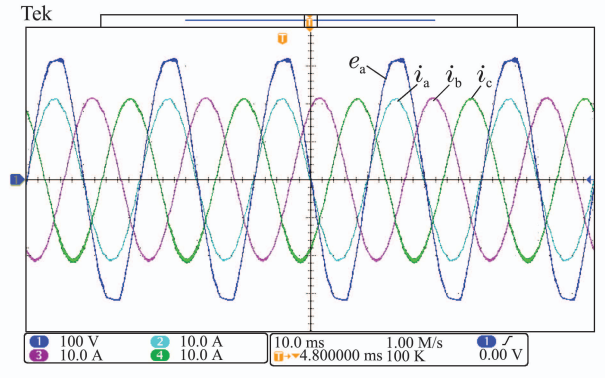

(b) Grid voltage e_a and input current

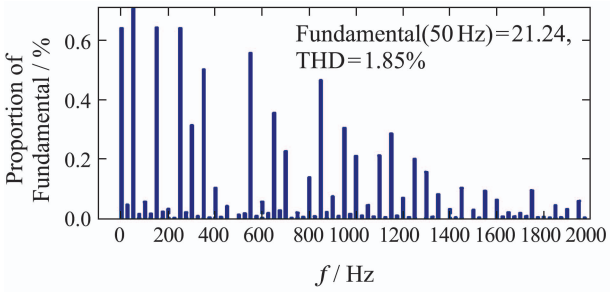

(c) FFT analysis of input current

Fig. 10 Experimental results of constrained MPC

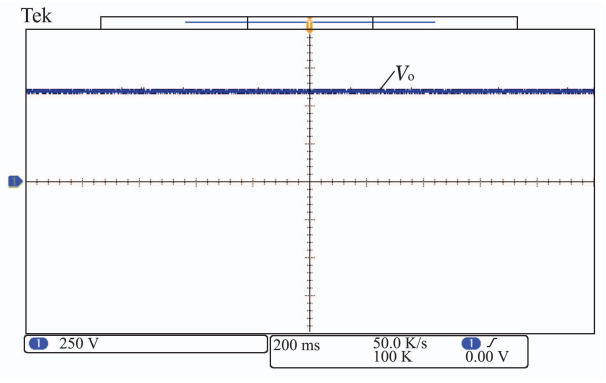

(a) Output DC voltage

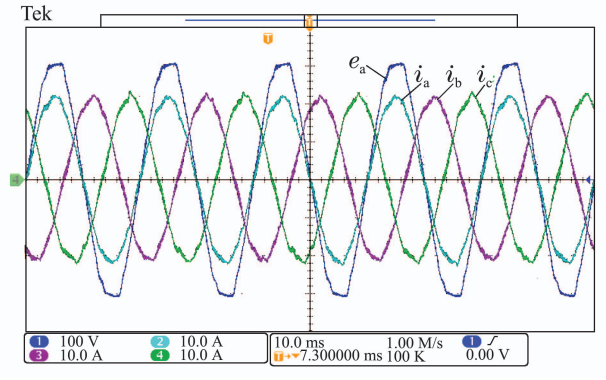

(b) Grid voltage e_a and input current

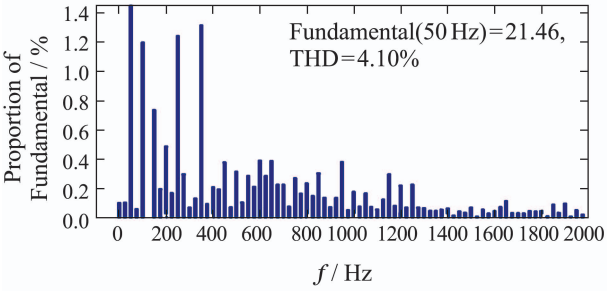

(c) FFT analysis of input current

Fig. 11 Experimental results of PI controller

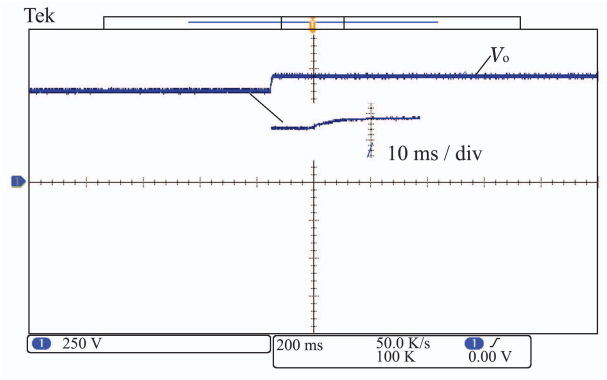

(a) Change reference DC voltage from 600 to 700

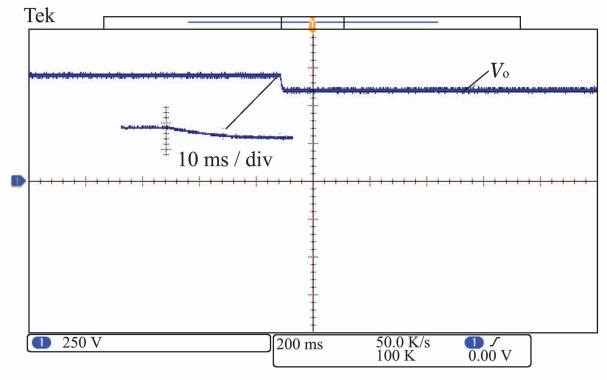

(b) Change reference DC voltage from 700 to 600

Fig. 12 Output DC voltage of constrained MPC

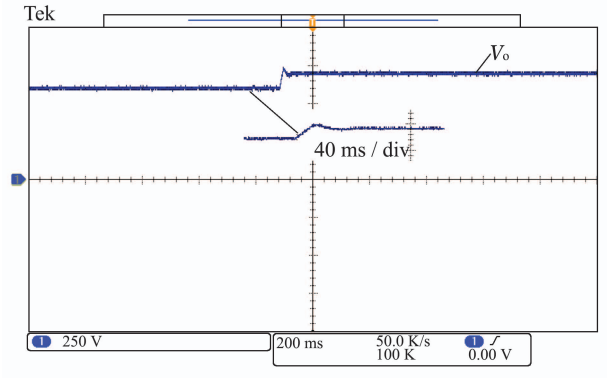

(a) Change reference DC voltage from 600 to 700

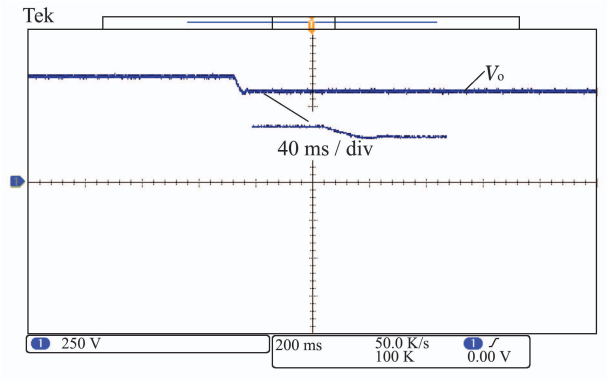

(b) Change reference DC voltage from 700 to 600

Fig. 13 Output DC voltage of PI controller

Compared with PI control, constrained MPC strategy decreases THD by 2.25%. After changing the reference value, the time to reach steady state again of constrained MPC is 12 ms, which is much shorter than that of PI controller, about 56 ms. The experimental results have demonstrated that the proposed constrained MPC strategy is feasible and achieves low THD and fast dynamic response.

5 Conclusions

In this paper, a constrained model predictive control strategy has been proposed for a three-phase PWM rectifier. Firstly, a decoupled model of the rectifier is built with no coordinate transformation and the discrete-time state-space equation is deduced. Then, the constrained MPC strategy is investigated and output-voltage loop control method is designed. Finally, simulation and experiment results verify effectiveness and feasibility of the constrained MPC strategy. According to the comparison between constrained MPC and PI control, it is found that constrained MPC can significantly improve stead state and dynamic performance of the rectifier. The measured THD is 2.5% lower and the time to reach steady state is 12 ms, which is one fifth of PI control.

Reference:

[1] ZHANG Y, YI Y, DONG P, et al. Simplified model and control strategy of three-phase PWM current source rectifiers for DC voltage power supply applications. *IEEE Journal of Emerging & Selected Topics in Power Electronics*, 2017, 3(4): 1090 – 1099.

[2] ZHANG W, HOU Y, LIU X, et al. Switched control of three-phase voltage source PWM rectifier under a wide-range rapidly varying active load. *IEEE Transactions on Power Electronics*, 2012, 27(2): 881 – 890.

[3] GUZMAN R, JOSE G D V L, MORALES J, et al. Sliding-mode control for a three-phase unity power factor rectifier operating at fixed switching frequency. *IEEE Transactions on Power Electronics*, 2016, 31(1): 758 – 769.

[4] CORTES P, KAZMIERKOWSKI M P, KENNEL R M, et al. Predictive control in power electronics and drives. *IEEE Transactions on Power Electronics*, 2008, 55(12): 4312 – 4324.

[5] VAZQUEZ S, RODRIGUEZ J, RIVERA M, et al. Model predictive control for power converters and drives. *IEEE Transactions on Industrial Electronics*, 2017, 64(2): 935 – 947.

[6] Bo, TORSTEIN I, JOHANSEN T A. Battery power smoothing control in a marine electric power plant using nonlinear model predictive control. *IEEE Transactions on Control Systems Technology*, 2017, 25(4): 1449 – 1456.

[7] LI Xiaoming, NIU Yuguang, WANG Shilin, et al. Adaptive neural decentralized-coordinated predictive control of double fed induction generator. *Control Theory & Applications*, 2015, 32(7): 902 – 911. (李晓明, 牛玉广, 王世林, 等. 双馈风机自适应神经分散协调预测控制. 控制理论与应用, 2015, 32(7): 902 – 911.)

[8] CHEN Q, LUO X, ZHANG L, et al. Model predictive control for three-phase four-leg grid-tied inverters. *IEEE Access*, 2017, 5(99): 2834 – 2841.

[9] LI Huijun, XIAO Bing. Multistep recurrent neural network model predictive controller without constraiints. *Control Theory & Applications*, 2012, 29(5): 642 – 648. (李会军, 肖兵. 一种无约束多步递归神经网络预测控制器. 控制理论与应用, 2012, 29(5): 642 – 648.)

[10] LI K, WAN J, GONG C, et al. An improved predictive current controlled three phase voltage PWM rectifier. *Innovative Smart Grid Technologies-asia*. Tianjin: IEEE, 2012, 5: 1 – 5.

[11] WANG J, NADEMI H, NORUM L. Control of input current harmonics and output voltage of three-phase voltage source PWM rectifier using model predictive control. *IEEE International Symposium on Industrial Electronics*. Taipei: IEEE, 2013, 5: 1 – 6.

[12] XIA C, WANG M, SONG Z, et al. Robust model predictive current control of three-phase voltage source PWM rectifier with online disturbance observation. *IEEE Transactions on Industrial Informatics*, 2012, 8(3): 459 – 471.

[13] CAI S, CAO H, LIANG D, et al. A three-phase voltage source PWM rectifier with strong DC immunity based on model predictive control. *Chinese Control Conference*. Hangzhou: CCC, 2015: 7871 – 7876.

[14] ZHANG Y, PENG Y, YANG H, et al. Performance improvement of two-vectors-based model predictive control of PWM rectifier. *IEEE Transactions on Power Electronics*, 2015, 31(8): 6016 – 6030.

[15] CORTES P, KOURO S, ROCCA B L, et al. Guidelines for weighting factors design in model predictive control of power converters and drives. *2009 IEEE International Conference on Industrial Technology*. Churchill: IEEE, 2009, 2: 1 – 7.

[16] SONG Z, TIAN Y, YAN Z, et al. Direct power control for three-phase two-level voltage-source rectifiers based on extended-state observation. *IEEE Transactions on Industrial Electronics*, 2016, 63(7): 4593 – 4603.

[17] ESKANDARI-TORBATI H, KHABURI D A. Direct power control of three phase PWM rectifier using model predictive control and SVM switching. *Power Electronics, Drive Systems & Technologies Conference*. Tehran: IEEE, 2013, 2: 193 – 198.

[18] JEREZ J L, GOULART P J, RICHTER S, et al. Embedded predictive control on an FPGA using the fast gradient method. *Control Conference*. Zurich: IEEE, 2013, 7: 3614 – 3620.

[19] JOAO F C M, JOAO M F X, AUIAR P M Q, et al. Distributed ADMM for model predictive control and congestion control. *IEEE Conference on Decision & Control*. Maui: IEEE, 2012, 12: 5110 – 5115.

作者简介:

刘 佳 硕士研究生, 目前研究方向为无线电能传输装置与控制, E-mail: 768292863@qq.com.cn;

张立炎 博士, 教授, 博士生导师, 目前研究方向为预测控制、车用新能源动力装置与控制和无线电能传输等, E-mail: zlywhut@whut.edu.cn;

陈启宏 教授, 博士生导师, 目前研究方向为新能源电力变换与控制和车用新能源动力装置与控制, E-mail: qh_chen@hotmail.com;

钱 立 硕士研究生, 目前研究方向为预测控制和电力电子变换与控制, E-mail: 1510882720@qq.com.cn;

全书海 教授, 博士生导师, 目前研究方向为模式识别与图像处理、智能信息处理和智能控制等, E-mail: quanshuh@whut.edu.cn.